Controlling entangled spin-orbit coupling of 5*d* states with interfacial heterostructure engineering

J.-W. Kim,[1] Y. Choi,[1] S. H. Chun,[2] D. Haskel,[1] D. Yi,[3] R. Ramesh,[4] J. Liu,[5] and P. J. Ryan[1]

[1]*Advanced Photon Source, Argonne National Laboratory, Argonne, Illinois 60439, USA*

[2]*Pohang Accelerator Laboratory, Pohang, Gyeongbuk 37673, Republic of Korea*

[3]*Department of Applied Physics, Stanford University, Stanford, California 94305, USA*

[4]*Department of Materials Science and Engineering, University of California, Berkeley, California 94720, USA*

[5]*Department of Physics and Astronomy, University of Tennessee, Knoxville, Tennessee 37996, USA*

(Received 16 January 2018; published 26 March 2018)

The combination of strong electron correlations in 3*d* transition-metal oxides and spin-orbit interactions in the 5*d* counterpart can give rise to exotic electronic and magnetic properties. Here, the nature of emerging phenomena at the interface between $SrIrO_3$ (SIO) and $La_{2/3}Sr_{1/3}MnO_3$ (LSMO) is presented. Nominally, SIO with strong spin-orbit interaction is metallic and nonmagnetic on the verge of a metal-insulator transition, whereas LSMO is metallic and ferromagnetic with itinerant character and high spin polarization. In the 1:1 LSMO/SIO superlattice, we observe ferromagnetic Mn moments with an insulating behavior, accompanied by antiferromagnetic ordering in SIO. Element-resolved x-ray magnetic circular dichroism proves that there is a weak net ferromagnetic Ir moment aligned antiparallel to the Mn counterpart. The branching ratio shows the formation of molecular orbitals between the Mn and Ir layers modifying the Ir 5*d* electronic configuration through the mixture of t_{2g} and e_g states, resulting in a deviation from $J_{\text{eff}} = 1/2$. This result demonstrates a pathway to manipulate the spin-orbit entanglement in 5*d* states with two-dimensional 3*d* spin-polarized electrons through heterostructure design.

DOI: 10.1103/PhysRevB.97.094426

The Mott insulating state in Sr_2IrO_4 has been a subject of considerable interest [1–4]. For Ir^{4+} in IrO_6 octahedra, the crystal field places five electrons in the t_{2g} *d*-state manifold and strong spin-orbit coupling in Ir^{4+} removes the orbital degeneracy by splitting the t_{2g} states into two effective angular momentum energy levels of filled $J_{\text{eff}} = 3/2$ and half-filled $J_{\text{eff}} = 1/2$ [1]. Consisting of two-dimensional IrO_2 layers, the structure of Sr_2IrO_4 resembles that of the La_2CuO_4 cuprate. In both the cuprates and iridates, the Mott insulating state with antiferromagnetic ordering is observed. These similarities lead to an interesting question whether Sr_2IrO_4, as a close analog to the undoped cuprate, can be modified to a superconducting state or other exotic states [2].

The electronic and magnetic ground states of the related iridate phases are highly tunable due to strong competition between spin-orbit and electron-electron interactions. Within the $Sr_{n+1}Ir_nO_{3n+1}$ Ruddlesden-Popper series, Sr_2IrO_4, Sr_3IrO_7, and $SrIrO_3$, as the number of neighboring Ir^{4+} atoms increases from 4, 5 to 6, the 5*d* bandwidth broadens modifying the ground state from Mott insulator, weak insulator to correlated metal, respectively [3]. In addition, the magnetic ground state is strongly influenced by the lattice geometry and anisotropic exchange coupling [4,5]. In $Sr_3Ir_2O_7$, doping with La^{3+} can induce a metallic state and reduce the magnetic ordering temperature [6]. Similarly, La^{3+} doping in Sr_2IrO_4 can induce a collapse of the Mott gap [7]. It has been shown that doping Sr_2IrO_4 with Mn, Ru, or Rh modifies the magnetic/electronic properties [8–12].

Thin-film heterostructures of perovskite oxide materials provide a fertile ground to study emergent interfacial behavior as structurally compatible materials with different properties are forced into contact in well-controlled two-dimensional structures. In thin $SrIrO_3$ (SIO) films the strain effect can induce a metal-insulator transition [13]. Superlattice structures of SIO and $SrTiO_3$ exhibit magnetic and electronic analogs to the $Sr_{n+1}Ir_nO_{3n+1}$ series [14]. At the interface with a ferromagnetic layer, a topological Hall effect was observed in bilayers of ferromagnetic $SrRuO_3$ and paramagnetic SIO through the Dzyaloshinskii-Moriya interaction [15]. Manipulation of magnetic anisotropy of 3*d* transition-metal oxides, LSMO is demonstrated by digitally inserting nonmagnetic SIO with spin-orbit coupling [16]. In thin films of (001)-oriented LSMO, the magnetization lies in the film plane with easy axis along [110] directions but the magnetic anisotropy of these LSMO films is typically weak [17,18]. In contrast, SIO thin films do not present any long-range magnetic ordering at least between 2 and 250 K [19]. Also, single-ion anisotropy is not anticipated in the pseudospin $J_{\text{eff}} = 1/2$ 5*d* state, since it gives the same quantized value for any direction, similar to spin $= 1/2$. Therefore, the evolution of the magnetic anisotropy should be related to the superlattice structure itself.

Among the superlattice family of $(LSMO)_m/(SIO)_n$, where m and n are the number of layers, the $m,n = 1$ system shows different behavior from the other members [16]. The temperature dependence of the resistivity exhibits insulating characteristics while each component in single-layer form is metallic [Fig. 1(a), inset]. The azimuthal magnetoresistance shows twofold symmetry [Fig. 1(b)] with magnetic easy axis along the [110] direction similar to the single-layer LSMO even though the interfacial effect is expected to be maximized in this film.

In this paper, we investigate the magnetic and electronic states of Ir 5*d* orbitals in $[(LSMO)_1/(SIO)_1]$ superlattice film. X-ray magnetic circular dichroism and x-ray resonant

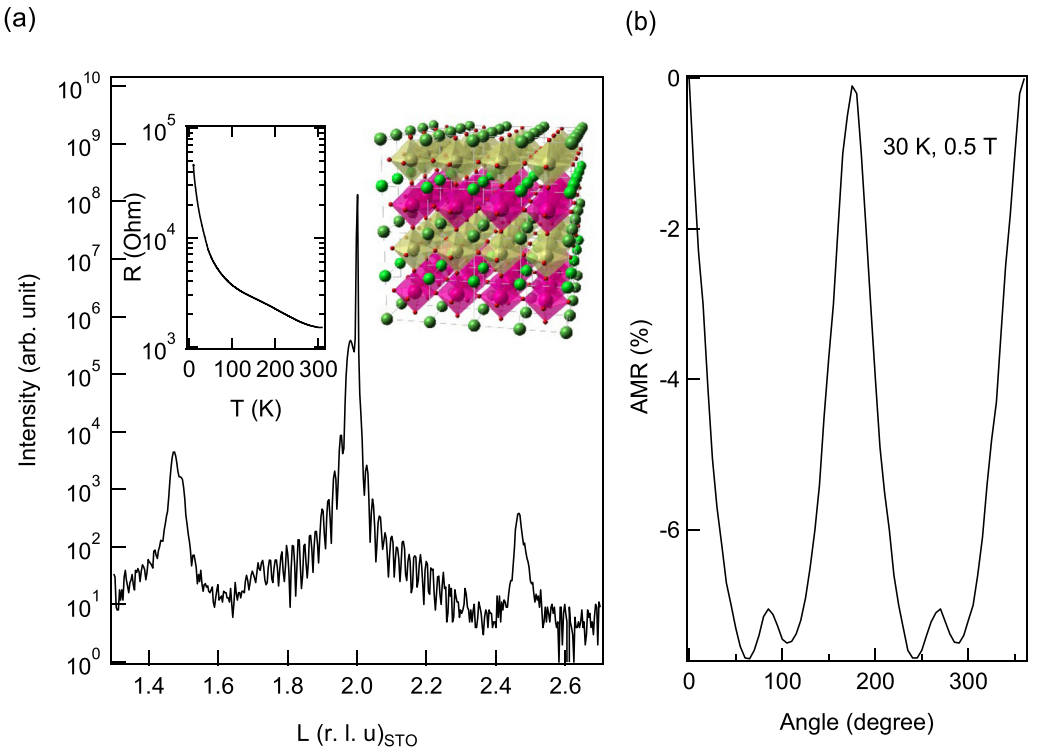

FIG. 1. (a) X-ray diffraction ($00L$) scan (out-of-plane direction of the film) shows film and superlattice peaks around the STO(002) substrate peak. (inset) Temperature dependence of resitivity shows the insulating behavior. Atomic structure of SIO/LSMO superlattice thin film is illustrated. (b) Azimuthal magnetic resistivity measured with 0.5 T at 30 K. The angle is zero when the magnetic field is along the [100] direction with respect to the STO structure.

magnetic scattering reveal the magnetic ordering of the Ir layer and its related spin-orbit coupling state. The isotropic and dichroic branching ratios (BRs) from x-ray absorption spectroscopy suggest the possible mixture of a crystal-field split state via the formation of molecular orbitals at the $3d$-$5d$ interface.

Using pulsed laser deposition, $[LSMO/SIO]_{x30}$ films were grown on (001)-oriented $SrTiO_3$ substrates. The bulk pseudocubic lattice parameters of LSMO, SIO, and $SrTiO_3$ (STO) are 3.876, 3.96, and 3.905 Å, respectively. The lattice mismatches correspond to about 1% in-plane tensile and compressive strain to LSMO and SIO, respectively. The film structure was characterized by x-ray diffraction, and magnetic properties were studied by a superconducting quantum interference device (SQUID). Electronic transport was characterized using a standard four-probe method in a physical property measurement system. To determine the magnetic structure of SIO, x-ray resonant magnetic spectroscopy and scattering at the Ir L edges were carried out at beamlines 4-ID-D and 6-ID-B of the Advanced Photon Source.

Figure 1(a) shows L scan around STO (002) reflection. The satellite peaks near $L = 1.5$ and 2.5 confirm the superstructure of SIO/LSMO layers. X-ray absorption near-edge structure (XANES) and x-ray magnetic circular dichroism (XMCD) measurements at the Ir $L_{3,2}$ edges are shown in Fig. 2. The branching ratio between the white-line intensities of L_2 and L_3, $\mathbf{BR} = \boldsymbol{I}_{L_3}/\boldsymbol{I}_{L_2}$, is related to the ground-state expectation value of the angular part of the spin-orbit coupling $\langle \boldsymbol{L} \cdot \boldsymbol{S} \rangle$ of the Ir $5d$ states, and deviation from the statistical BR = 2 indicates strong spin-orbit interaction [20]. In comparison with the results from Sr_2IrO_4 powder samples [21], the Ir L_3 absorption edge position is nearly identical, which supports that the iridium oxidation in the LSMO/SIO is close to Ir^{4+}. In contrast to a BR = 4.1 in the powder sample, the white-line intensities are reduced by 8 and 15%, respectively, for the Ir L_3 and L_2 edges so that the branching ratio is about 8% larger in the LSMO/SIO, leading to a BR = 4.4. This result implies that the spin-orbit coupling value $\langle \boldsymbol{L} \cdot \boldsymbol{S} \rangle$ is larger due to the e_g contribution to the $5d$ orbital state.

The net moment along the field direction is measured by XMCD, and employing sum rules provides information on the expectation values of spin and orbital moments, $\langle S_z \rangle$ and $\langle L_z \rangle$ [22]. Here the orbital and spin moments are parallel to each other, but their directions are opposite to the magnetic-field direction. The orientation was verified independently by measuring a Sr_2IrO_4 powder sample in transmission and fluorescence modes using the same experimental setup. As shown in Fig. 2, the LSMO/SIO gives opposite Ir L_3 XMCD signal in comparison with the Sr_2IrO_4 case, where the net Ir moment (canted AFM moment) is along the field direction. This shows that the net Ir moment is antiparallel to the Mn moment in the adjacent LSMO layers. Similarly, in the $3d/4d$ perovskite heterostructure between LSMO and $SrRuO_3$, an interfacial antiferromagnetic coupling was observed between the constituent layers due to the hybridization of O $2p$ with both Mn $3d$ and Ru $4d$ states [23]. With five holes in the Ir $5d$ orbital, sum rules analysis gives $\langle L_z \rangle = -0.053\,\mu$B/Ir and $\langle S_z \rangle + 7/2\langle T_z \rangle = -0.0113\,\mu_B$/Ir, where $\langle T_z \rangle$ is the magnetic

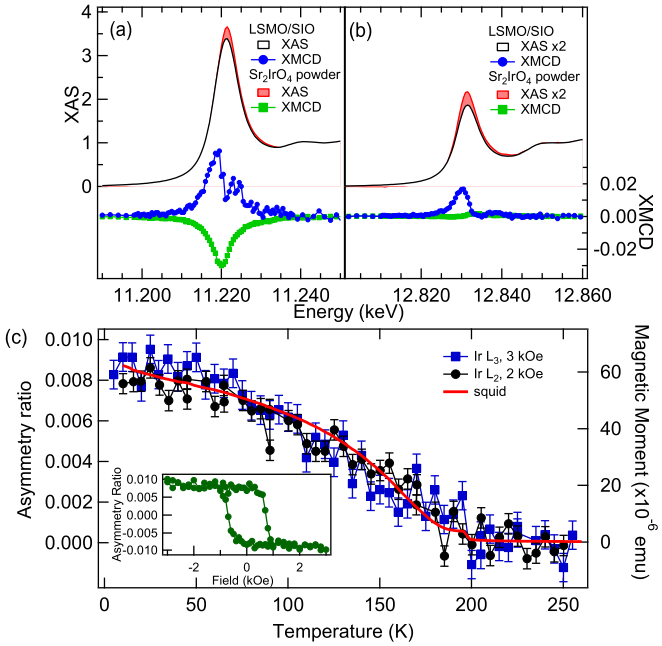

FIG. 2. (a), (b) X-ray absorption spectra and x-ray magnetic circular dichroism at the Ir $L_{2,3}$ edges from the LSMO/SIO and Sr_2IrO_4 reference sample. Compared with the Sr_2IrO_4 reference sample, the white-line intensity decreases in both L_2 and L_3. The relative reduction of the white-line intensity is larger in L_2 than L_3 (the difference is shaded light red), indicating that the isotropic branching ratio is larger in LSMO/SIO film than Sr_2IrO_4 bulk. (c) Temperature dependence of Ir $L_{2,3}$ XMCD signal. Asymmetry ratio is defined here as $(I^+ - I^-)/(I^+ + I^-)$, where I^+, I^- are the absorption intensities for opposite helicity of the circularly polarized x rays. The inset shows the field dependence of the Ir L_3 asymmetry ratio at 5 K.

dipole term describing the anisotropy of the spin density in the material. While the $\langle T_z \rangle$ term can be neglected in the case for cubic $3d$ transition metals, it may not be negligible with strong crystal-field or spin-orbit effects in heavy elements [24,25]. The $\langle T_z \rangle$ term is not easily measured nor estimated from band-structure calculations. The ideal $J_{\text{eff}} = 1/2$ case gives $\langle L_z \rangle / \langle S_z \rangle = (2/3)/(1/6) = 4$ [26]. In the current LSMO/SIO case, neglecting $\langle T_z \rangle$ in our XMCD sum rules analysis gives $\langle L_z \rangle / \langle S_z \rangle = 4.4$, and this value is likely an underestimate. For example, including the $\langle T_z \rangle$ value from the $BaIrO_3$ case [25] leads to 7.3. In a recent nonresonant magnetic x-ray diffraction study, $\langle L_z \rangle / \langle S_z \rangle = 5.0$ was reported and the enhanced ratio was attributed to a significant hybridization of the $J_{\text{eff}} = 1/2$ with other orbital states rather than to a small tetragonal distortion in a Sr_2IrO_4 single crystal [27].

In Fig. 2, the Ir L_2 XMCD of the LSMO/SIO film is significantly larger than that of Sr_2IrO_4 [21]. This suggests the present case deviates from the exact $J_{\text{eff}} = 1/2$ state realized in the cubic symmetry. Within the LSMO/SIO structure, the SIO layers are under compressive, in-plane strain which possibly makes the tetragonal crystal-field effect significant. Charge transfer (CT) across the interface might be expected to play a role, but both the XANES and insulating behavior suggest that it does not. Here, we apply a single-ion model, treating the spin-orbit interaction $\xi \langle L \cdot S \rangle$ and tetragonal crystal-field terms Δ to our XMCD result [28]. For the ideal cubic symmetry case, the strong spin-orbit coupling drives the $Ir^{4+}(5d^5)$ into the $J_{\text{eff}} = 1/2$ state in which the hole-xy, yz, and zx states are equally unoccupied with specific spin combinations. Therefore, the hole state can be written in the following form:

$$|0,+\rangle = \frac{C_0|xy,-\rangle + |yz,+\rangle - i|zx,+\rangle}{\sqrt{2+C_0}}$$

This is the same representation as the deformed wave function by tetragonal crystal-field effect of the apical distortion where $2C_0 = \delta - 1 + \sqrt{9 + \delta(\delta - 2)}$ and $\delta = 2\Delta/\xi$ [28]. When C_0 is larger than 1 the hole state would have more in-plane character, and vice versa. Based on this model the XMCD branching ratio is calculated as below.

$$\text{XMCD}(L_2/L_3) = (C_0 - 1)^2/\left(2 + 2C_0 - C_0{}^2\right).$$

The measured branching ratio is $\sim 1/3$ so that $C_0 = \sim 1.866$ or 0.134. According to C_0 the ratio of axial distortion energy and spin-orbit coupling coefficient Δ/ξ is 0.8972 or -6.895. Both values are too large for the expected uniaxial distortion energy. Hence, these results do not explain this hole state simply with uniaxial distortion only. The induced ferromagnetic component from the Ir atoms is influenced by magnetically polarized electrons from the Mn layer. Hybridizing e_g states of Ir and Mn lobes by the formation of molecular orbitals brings the e_g character of the Ir $5d$ states below the Fermi level [29]. As mentioned above, the x-ray absorption spectroscopy (XAS) isotropic branching ratio is also consistent with this model of intermixing t_{2g} and e_g since no CT at the interface was observed in this system [16]. As a result of the combination of various conditions, the induced net moment of Ir layers differs from $J_{\text{eff}} = 1/2$.

Temperature dependence of the Ir $L_{2,3}$ XMCD is presented in comparison to SQUID magnetometry in Fig. 2(c). The $L_{2,3}$ absorption edges show the same temperature dependence, indicating the XMCD branching ratio is constant. At both edges, the XMCD signals persist nearly up to 180 K. While the Ir XMCD result is sensitive to the Ir moment only, the SQUID data are sensitive to the overall moment from the sample. However, considering the net Mn moment is expected to be an order of magnitude larger than the net Ir moment, the SQUID result mostly represents the response of the LSMO layers. The Ir XMCD and SQUID show similar temperature dependence, indicating that the Ir XMCD is induced by the Mn moments forming the molecular orbitals.

To probe the antiferromagnetic components of the Ir ions, we carried out x-ray magnetic resonant-scattering measurements. The x-ray energy was tuned at the Ir L edges to enhance the Ir magnetic response [Fig. 3(b), inset]. The polarization analysis of σ-π geometry is achieved by a pyrolytic graphite (008) polarization analyzer. The presence of a peak around $(0.5\,0.5\,L)_{\text{STO}}$ (L is an integer of $SrTiO_3$ reciprocal lattice units) and resonant enhancement at the Ir L_3 edge indicates this reflection is from Ir magnetic scattering. Thus, a magnetic structure with the simple checkerboard-type AFM ordering in the SIO layer repeats the identical order to the other SIO layers [Fig. 3(a)]. The temperature dependence of the magnetic scattering intensity of AFM order is consistent with Mn moment square (M^2) by SQUID [Fig. 3(b)]. This suggests that the LSMO ferromagnetism mediates the interaction between the antiferromagnetic SIO layers.

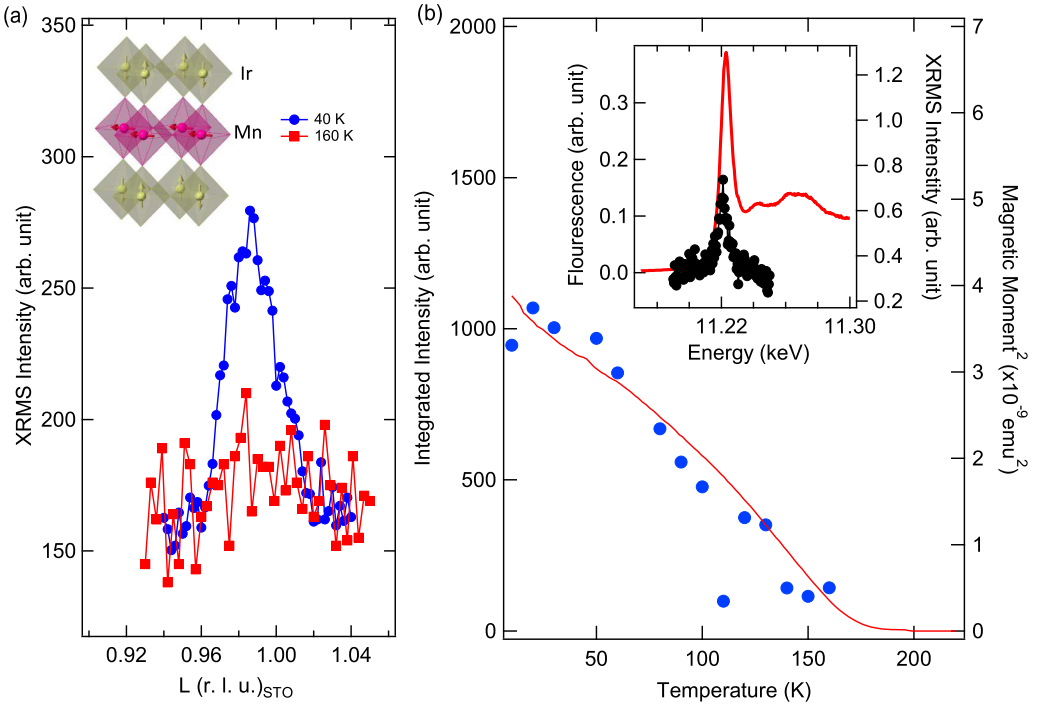

FIG. 3. (a) Magnetic scattering intensity around (0.5 0.5 1) position at 40 and 160 K. The inset shows the magnetic structure of the superlattice film. The AFM order of Ir moments corresponds to the (0.5 0.5 L) magnetic reflection with the FM Mn layer. (b) Temperature dependence of magnetic scattering intensity at (0.5 0.5 1) compared with magnetization square (M^2) measured by SQUID. The resonant enhancement of the magnetic intensity across the Ir L_3 edge is shown in the inset.

In Fig. 4, the magnetic-field dependence of the $(0.5\ 0.5\ 1)_{pc}$ AFM peaks is presented in order to show the correlation between the ferromagnetic Mn and antiferromagnetic Ir order. A decrease of AFM intensity is observed at the coercive fields [Fig. 4(c), inset]. Here, the ferromagnetic Mn order divides into domains with various orientations resulting in a net zero Mn moment. Since the magnetic scattering intensity is directly related to the Ir moment direction of the AFM ordering, the intensity minima suggest that the AFM order also develops domains with different moment directions. In

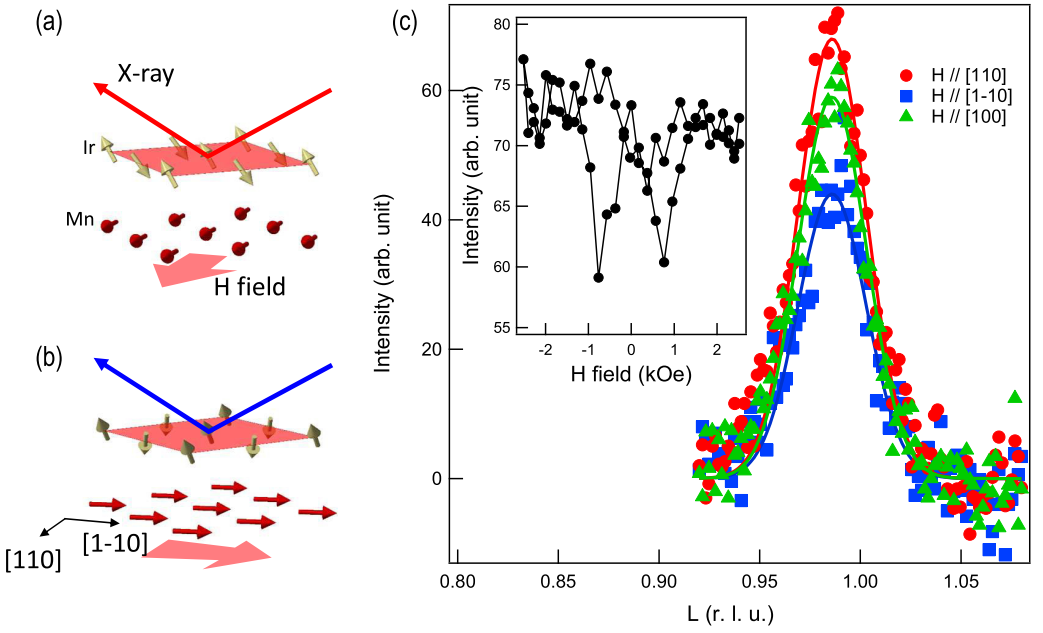

FIG. 4. The scattering geometry and magnetic moment alignment when H field is applied along [110] direction (a) and [1-10] direction (b). (c) L scans of (0.5 0.5 1) magnetic peak with different magnetic-field directions. Inset shows the change of (0.5 0.5 1) magnetic peak intensity as a function of magnetic field, H//[110].

order to verify this supposition, the AFM peak intensity is examined with Mn moments aligned to particular directions. Due to the large remanence (close to the saturated moment), the magnetic scattering intensity is measured at zero field after the field is applied having aligned the moments along three in-plane directions, [110], [1-10], and [100]. It shows maximum scattering intensity when the Mn moment is along the [110] direction and minimum intensity along the [1-10] direction [Fig. 4(c)]. The [100] direction represents the average intensity between [110] and [1-10]. Therefore, the intensity minima at the coercive field during the field sweeping demonstrates how the randomly oriented Ir AFM domain structure is coupled to the Mn moment direction.

The x-ray resonant magnetic scattering (XRMS) with magnetic-field measurements confirm that the Ir AFM order is coupled to the Mn moment. A possible magnetic configuration would be the ferromagnetic Mn spin being perpendicular to the Ir AFM moment, since in this configuration a slight canting of Ir moments leads to the weak ferromagnetic component opposite to the Mn spin direction and this may lower the overall magnetic interaction energy. From the SQUID measurement it is established that the easy axis of Mn moment is in-plane; therefore, AFM Ir moments perpendicular to the Mn would be either within the plane, out of plane, or between the two directions. In the case that the AFM Ir moments are within the plane, the AFM intensity difference estimated from the magnetic resonant scattering cross section $(\widehat{k'} \cdot \vec{m})^2$ should be about 100 times greater than either between the Mn moments aligned along [1-10] or the [110] direction. On the other hand, when the AFM Ir moments are along the film normal, there should be no difference in XRMS intensity with respect to the Mn moment direction. The experimental result shows that the intensity ratio between the [1-10] and [110] directions is about 0.6, which indicates that the AFM moment contains both in- and out-of-plane components [Figs. 4(a) and 4(b)].

The variation of the magnetic scattering intensity is relatively small so that the AFM moment direction is mostly along the out-of-plane direction. Tilting of AFM order from the surface normal is estimated to be about 6° assuming equal domain distribution [30]. This is consistent with the spin orientation of the Mn-doped Sr_2IrO_4 and furthermore, relevant to the topological Hall effect at the $3d$-$5d$ interface demonstrated in the $SrRuO_3/SrIrO_3$ superlattice thin films [15].

In conclusion, with a $[SIO/LSMO]_{x\,30}$ perovskite superlattice structure, we observe the reconstruction of two-dimensional electronic and magnetic states via the $3d$-$5d$ interface interaction. Large XMCD signal at the Ir L_2 edge indicates that the induced Ir moment deviates from the $J_{\text{eff}} = 1/2$ state. Magnetically polarized electrons from the Mn layer alter the orbital configuration of the Ir $5d$ state. The XAS branching ratio change suggests that the mixture of t_{2g} and e_g states is due to the formation of molecular orbitals between the Mn and Ir layers. X-ray resonant magnetic scattering at the Ir L_3 edge reveals that the modified $5d$ state in the SIO layer develops AFM ordering with the magnetic moment direction out of the film plane. This study demonstrates that tuning the spin-orbit entanglement within correlated electron systems with two-dimensional interfacial effects employing heterolayer structure design may be a promising approach in realizing new electronic, magnetic, and topological phases.

This research used resources of the Advanced Photon Source, a U.S. Department of Energy (DOE) Office of Science User Facility operated for the DOE Office of Science by Argonne National Laboratory under Contract No. DE-AC02-06CH11357. The work at Berkeley was supported by the Director, Office of Science, Office of Basic Energy Sciences, of the US Department of Energy under Contract No. DE-AC02-05CH11231 under the Quantum Materials program.

[1] B. J. Kim, H. Jin, S. J. Moon, J.-Y. Kim, B.-G. Park, C. S. Leem, J. Yu, T. W. Noh, C. Kim, S.-J. Oh, J.-H. Park, V. Durairaj, G. Cao, and E. Rotenberg, Novel $J_{\text{eff}} = 1/2$ Mott State Induced by Relativistic Spin-Orbit Coupling in Sr_2IrO_4, Phys. Rev. Lett. **101**, 076402 (2008).

[2] Y. K. Kim, O. Krupin, J. D. Denlinger, A. Bostwick, E. Rotenberg, Q. Zhao, J. F. Mitchell, J. W. Allen, and B. J. Kim, Fermi arcs in a doped pseudospin-1/2 Heisenberg antiferromagnet, Science, **345**, 187 (2014).

[3] S. J. Moon, H. Jin, K. W. Kim, W. S. Choi, Y. S. Lee, J. Yu, G. Cao, A. Sumi, H. Kunakubo, C. Bernhard, and T. W. Noh, Dimensionality-Controlled Insulator-Metal Transition and Correlated Metallic State in 5d Transition Metal Oxides $Sr_{n+1}Ir_nO_{3n+1}$ ($n = 1,2$, and ∞), Phys. Rev. Lett. **101**, 226402 (2008).

[4] G. Jackeli and G. Khaliullin, Mott Insulators in the Strong Spin-Orbit Coupling Limit: From Heisenberg to a Quantum Compass and Kitaev Models, Phys. Rev. Lett. **102**, 017205 (2009).

[5] J. W. Kim, Y. Choi, J. Kim, J. F. Mitchell, G. Jackeli, M. Daghofer, J. van den Brink, G. Khaliullin, and B. J. Kim, Dimensionality Driven Spin-Flop Transition in Layered Iridates, Phys. Rev. Lett. **109**, 037204 (2012).

[6] L. Li, P. P. Kong, T. F. Qi, C. Q. Jin, S. J. Yuan, L. E. DeLong, P. Schlottmann, and G. Cao, Tuning the $J_{\text{eff}} = 1/2$ insulating state via electron doping and pressure in the double-layered iridate $Sr_3Ir_2O_7$, Phys. Rev. B **87**, 235127 (2013).

[7] A. de la Torre, S. McKeown Walker, F. Y. Bruno, S. Ricco, Z. Wang, I. Gutierrez Lezama, G. Scheerer, G. Giriat, D. Jaccard, C. Berthod, T. K. Kim, M. Hoesch, E. C. Hunter, R. S. Perry, A. Tamai, and F. Baumberger, Collapse of the Mott Gap and Emergence of a Nodal Liquid in Lightly Doped Sr_2IrO_4, Phys. Rev. Lett. **115**, 176402 (2015).

[8] S. Calder, G.-X. Cao, M. D. Lumsden, J. W. Kim, Z. Gai, B. C. Sales, D. Mandrus, and A. D. Christianson, Magnetic structural change of Sr_2IrO_4upon Mn doping, Phys. Rev. B **86**, 220403(R) (2012).

[9] J. P. Clancy, A. Lupascu, H. Gretarsson, Z. Islam, Y. F. Hu, D. Casa, C. S. Nelson, S. C. LaMarra, G. Cao, and Y.-J. Kim, Dilute magnetism and spin-orbital percolation effects in $Sr_2Ir_{1-x}Rh_xO_4$, Phys. Rev. B, **89**, 054409 (2014).

[10] C. Dhital, T. Hogan, W. Zhou, X. Chen, Z. Ren, M. Pokharel, Y. Okada, M. Heine, W. Tian, Z. Yamani, C. Opeil, J. S. Helton, J. W. Lynn, Z. Wang, V. Madhavan, and S. D. Wilson, Nat. Commun. **5**, 3377 (2014).

[11] A. Glamazda, W.-J. Lee, K.-Y. Choi, P. Lemmens, H. Y. Choi, N. Lee, and Y. J. Choi, Effects of hole doping on magnetic and lattice excitations in $Sr_2Ir_{1-x}Ru_xO_4(x = 0–0.2)$, Phys. Rev. B **89**, 104406 (2014).

[12] T. F. Qi, O. B. Korneta, L. Li, K. Butrouna, V. S. Cao, X. Wan, P. Schlottmann, R. K. Kaul, and G. Cao, Spin-orbit tuned metal-insulator transitions in single-crystal $Sr_2Ir_{1-x}Rh_xO_4(0 < x < 1)$, Phys. Rev. B **86**, 125105 (2012).

[13] J. H. Gruenewald, J. Nichols, J. Terzik, G. Cao, J. W. Brill, and S. S. A. Seo, Compressive strain-induced metal–insulator transition in orthorhombic $SrIrO_3$ thin films, J. Mater. Res., **29**, 2491 (2014).

[14] J. Matsuno, K. Ihara, S. Yamamura, H. Wadati, K. Ishii, V. V. Shankar, H.-Y. Kee, and H. Takagi, Engineering Spin-Orbit Magnetic Insulator by Tailoring Superlattices, Phys. Rev. Lett. **114**, 247209 (2015).

[15] J. Matsuno, N. Ogawa, K. Yasuda, F. Kagawa, W. Koshibae, N. Nagaosa, Y. Tokura, and M. Kawasaki, Interface-driven topological Hall effect in $SrRuO_3$-$SrIrO_3$ bilayer, Sci. Adv. **2**, e1600304 (2016).

[16] D. Yi, J. Liu, S.-L. Hsu, L. Zhang, Y. Choi, J.-W. Kim, Z. Chen, J. D. Clarkson, C. R. Serrao, E. Arenholz, P. J. Ryan, H. Xu, R. J. Birgeneau, and R. Ramesh, Atomic-scale control of magnetic anisotropy via novel spin–orbit coupling effect in $La_{2/3}Sr_{1/3}MnO_3/SrIrO_3$ superlattices, Proc. Natl. Acad. Sci. U.S.A. **113**, 6397 (2016).

[17] L. M. Berndt, V. Blbarin, and Y. Suzuki, Magnetic anisotropy and strain states of (001) and (110) colossal magnetoresistance thin films, Appl. Phys. Lett. **77**, 2903 (2000).

[18] M. Konoto, T. Kohashi, K. Koike, T. Arima, Y. Kaneko, Y. Tomioka, and Y. Tokura, Magnetic domain structure of a $La_{0.7}Sr_{0.3}MnO_3$ (001) surface observed by a spin-polarized scanning electron microscope, Appl. Phys. Lett. **84**, 2361 (2004).

[19] M. Miyazaki, R. Kadono, M. Hiraishi, A. Koda, K. M. Kojima, K. Ohashi, T. Takayama, and H. Takagi, Evidence for ordered magnetic moments at oxygen sites in antiferromagnetic Sr_2IrO_4 and $Sr_3Ir_2O_7$, Phys. Rev. B **91**, 155113 (2015).

[20] G. van der Laan and B. T. Thole, Local Probe for Spin-Orbit Interaction, Phys. Rev. Lett. **60**, 1977 (1988).

[21] D. Haskel, G. Fabbris, M. Zhernenkov, P. P. Kong, C. Q. Jin, G. Cao, and M. van Veenendaal, Pressure Tuning of the Spin-Orbit Coupled Ground State in Sr_2IrO_4, Phys. Rev. Lett. **109**, 027204 (2012).

[22] P. Carra, B. T. Thole, M. Altarelli, and X. Wang, X-Ray Circular Dichroism and Local Magnetic Fields, Phys. Rev. Lett. **70**, 694 (1993).

[23] M. Ziese, I. Vrejoiu, E. Pippel, P. Esquinazi, D. Hesse, C. Etz, J. Henk, A. Ernst, I. V. Maznichenko, W. Hergert, and I. Mertig, Tailoring Magnetic Interlayer Coupling in $La_{0.7}Sr_{0.3}MnO_3$-$SrRuO_3$ Superlattices, Phys. Rev. Lett. **104**, 167203 (2010).

[24] S. P. Collins, D. Laundy, C. C. Tang, and G. van der Laan, An investigation of uranium $M_{4,5}$ edge magnetic x-ray circular dichroism in US, J. Phys. Condens. Matter **7**, 9325 (1995).

[25] M. A. Laguna-Marco, D. Haskel, N. Souza-Neto, J. C. Lang, V. V. Krishnamurthy, S. Chikara, G. Cao, and M. van Veenendaal, Orbital Magnetism and Spin-Orbit Effects in The Electronic Structure of $BaIrO_3$, Phys. Rev. Lett. **105**, 216407 (2010).

[26] B. J. Kim, H. Ohsumi, T. Komesu, S. Sakai, T. Morita, H. Takagi, and T. Arima, Phase-sensitive observation of a spin-orbital Mott state in Sr_2IrO_4, Science **323**, 1329 (2009).

[27] S. Fujiyama, H. Ohsumi, K. Ohashi, D. Hirai, B. J. Kim, T. Arima, M. Takata, and H. Takagi, Spin and Orbital Contributions to Magnetically Ordered Moments in 5d Layered Perovskite Sr_2IrO_4, Phys. Rev. Lett. **112**, 016405 (2014).

[28] M. Moretti Sala, S. Boseggia, D. F. McMorrow, and G. Monaco, Resonant X-Ray Scattering and The $j_{\text{eff}} = 1/2$ Electronic Ground State in Iridate Perovskites, Phys. Rev. Lett. **112**, 026403 (2014).

[29] S. Okamoto, J. Nichols, C. Sohn, S. Y. Kim, T. W. Noh, and H. N. Lee, Charge transfer in iridate-manganite superlattices, Nano Lett. **17**, 2126 (2017).

[30] Tilting the AFM order from the surface normal direction results in the in-plane AFM component which is independent from the canted FM order opposite to the Mn spins.